Article:
Pérez-Urquizo, J, Todorov, Y, Li, L orcid.org/0000-0003-4998-7259 et al. (5 more authors) (2021) Monolithic Patch-Antenna THz Lasers with Extremely Low Beam Divergence and Polarization Control. ACS Photonics, 8 (2). pp. 412-417. ISSN 2330-4022

https://doi.org/10.1021/acsphotonics.0c01430

Monolithic patch-antenna THz lasers with extremely low beam divergence and polarization control.

Joel Pérez-Urquizo,[1] Yanko Todorov,[2] Lianhe Li,[3] Alexander G. Davies,[3] Edmund H. Linfield,[3] Carlo Sirtori,[2] Julien Madéo,[1,*] and Keshav M. Dani[1].

[1]Femtosecond Spectroscopy Unit, Okinawa Institute of Science and Technology Graduate University, Onna-son, Okinawa 904-0495, Japan.

[2]Laboratoire de Physique de l'Ecole Normale Supérieure ENS, Université PSL, CNRS, Université de Paris, Sorbone Paris Cité Paris, France.

[3]School of Electronic and Electrical Engineering, University of Leeds, Leeds, LS2 9JT, United Kingdom.

Supporting Information Placeholder

ABSTRACT: Arrays of patch antennas have impacted modern telecommunications in the RF range significantly, owing to their versatility in tailoring the properties of the emitted radiation such as beam width and polarization, along with their ease of fabrication. At higher frequencies, in the terahertz (THz) range, there is a pressing need for a similar monolithic platform to realize and enable the advanced functionalities available in RF technology. This platform would benefit a wide variety of fields such as astronomy, spectroscopy, wireless communications and imaging. Here, we demonstrate THz lasers made of arrays of 10 X 10 patch antenna microcavities that provide up to 25 mW output power with robust single mode frequency and spatial mode. This device architecture leads to an unprecedented beam divergence, better than 2°x2°, which depends only on the number of resonators. This allows to functionalize the device while preserving a high quality far-field pattern. By interconnecting the symmetric square microcavities with narrow plasmonic wires along one direction, we introduce an asymmetry into the originally degenerate and cross-polarized TM_{01} and TM_{10} modes, leading to a precise control of the resonant frequency detuning between the TM modes. This feature allows devices to be designed that radiate with any coherent polarization states from linear to circular. Large-scale full-wave simulations of the emission from entire arrays support our experimental results. Our platform provides a solution to finally achieve monolithic terahertz emitters with advanced integrated functionalities such as active beam steering and polarization control.

KEYWORDS: THz QCL, patch-antenna microcavities, surface emission, beam shaping, coherent polarization control,

The prevailing methodology in the radiofrequency (RF) band for shaping and sending usable electromagnetic radiation into free space has been the use of antenna phased-arrays. In particular, microstrip patch antennas [1] have been extensively exploited and are currently implemented in modern 5G communications technologies owing to their compact size, easy tunability, and full compatibility with planar fabrication techniques [2, 3]. In the THz domain, patch antenna arrays have been used for fundamental studies of the ultra-strong light-matter coupling regime [4], for phase-shaping metamaterials [5], and as perfect absorbers [6]. Functionalizing such arrays with electrical inputs to create practical devices without hindering their optical properties is a non-trivial problem, as demonstrated in this work. Recently, arrays of patch antennas that acted also as microcavities (by substituting the usual dielectric medium with active semiconductor heterostructures) were demonstrated to function as high performance detectors in the mid-infrared range with room temperature operation [7] and with detectivity levels comparable to commercial bolometers in the THz range [8]. This success originates from the ability of patch antenna microcavities to combine the advantage of a strong subwavelength mode confinement with efficient light harvesting from their antenna [9-11]. However, questions remain about the relevance of using this structure for emission in the THz range due to low quality factors [12, 13] and high beam divergence [14, 15], as such, only electroluminescence has been reported [16, 17]. To date, lasing emission has been observed only through the use of an external cavity [18-20] and when used as passive out-couplers in association with ridge waveguide lasers [15], but a monolithic solution remains elusive. In this letter, we report efficient lasing at 3.2 THz from an array of patch antenna microcavities connected by narrow plasmonic wires. First, we show that a wired array of patch microcavities radiates like a phased-array to achieve beam shaping, and second, we demonstrate that the desired polarization state can be produced by engineering the array and wire dimensions.

Results

Figure 1 (a) presents the structure of the studied and fabricated arrays comprising 100 patch elements containing a quantum cascade laser (QCL) active region, arranged in a 10x10 planar configuration. Details about the fabrication process are presented in the Methods section. As shown in our previous numerical work [21], periodic arrays formed by a large number of patch resonators provide enhanced quality factors compared to the low-Q single resonator allowing self lasing from the patch.

The square microresonators are connected along one direction by subwavelength wires of length d and width of 2 µm. The microcavities have their resonance condition determined by the patch size s according to $s = \lambda/2n_{eff}$, where n_{eff} is the effective mode index and λ the emission wavelength. We performed full-wave finite element simulations of 10x10 phase-locked arrays to investigate their emission. As expected from patch antennas, the emission is normal to the surface (Figure 1 (a)) as the polarization of the radiation, originating from the fringing fields located at the edges of the resonators, rotates by 90° with respect to the intracavity TM mode when out-coupling to free space [22] . Their emission undergoes successive interference leading to the constructive formation of a narrow beam in the far-field (Figure 1 (a)-bottom panel).

In general, a square patch antenna supports the degenerate fundamental modes TM_{10} and TM_{01}, whose field distribution is given by $E_{z0}\cos\left(\frac{\pi}{s}x\right)$ and $E_{z0}\sin\left(\frac{\pi}{s}y\right)$, respectively [22]. Figure 1 (b) shows the electric field distribution for the TM_{10} and TM_{01} modes, and the effect on the TM_{01} mode of the addition of the 2-µm-wide wires. The TM_{10} mode resonant frequency and quality factor remain unaffected compared to a bare patch (no wires, see Figure 1

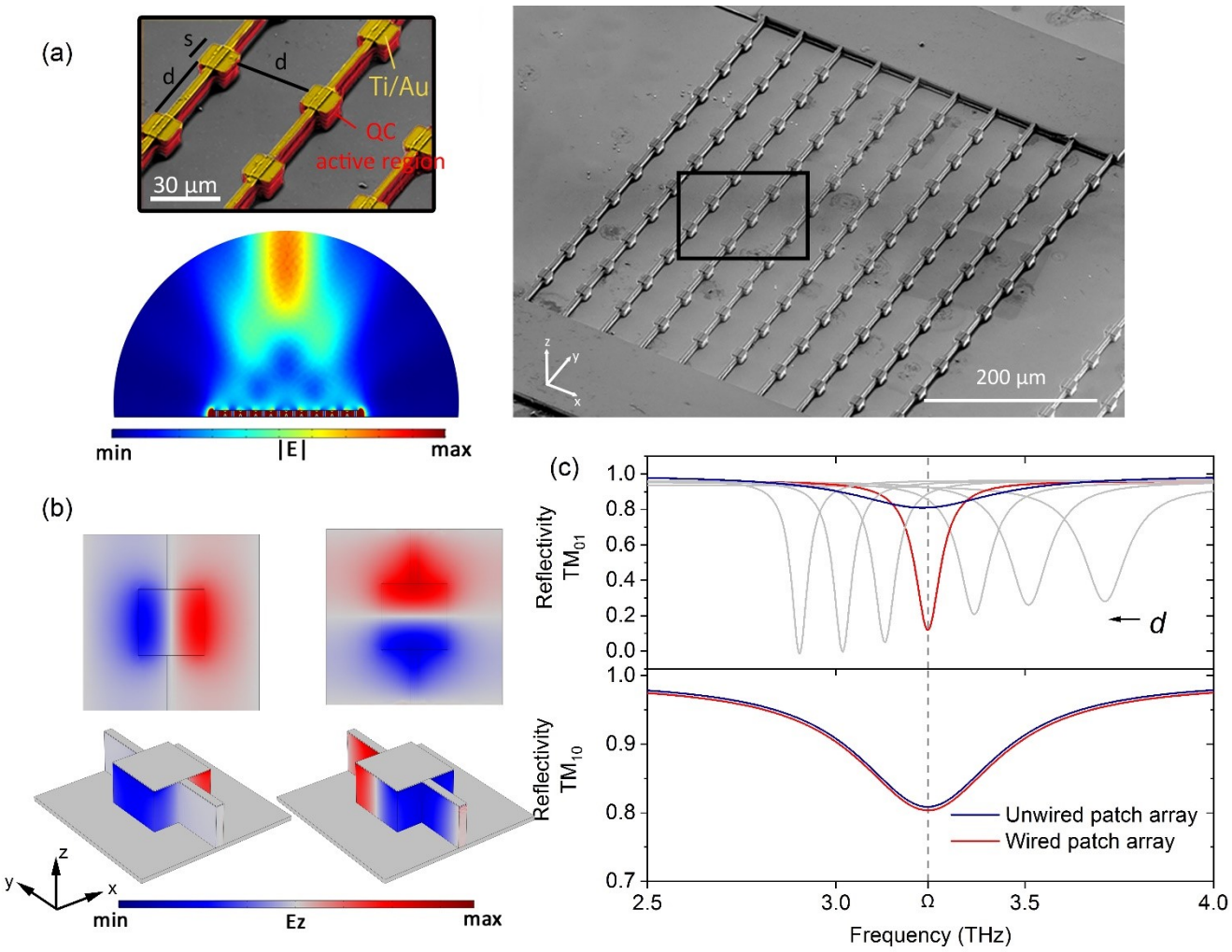

Figure 1. (a) (Left top and right) Scanning electron microscope image of a fabricated device. The array consists of 100 patch-antenna elements of width *s* interconnected by thin wires of length *d*, arranged in a 10x10 planar array. The current bias is injected into the device through rectangular contact pads positioned at the top and bottom of the array and insulated from the QC active region by a 200-nm-thick SiO_2 layer. (Left bottom) Finite element simulation of the radiation from a 10x10 array (a cross section of the 3D model is shown). Color scale represents the amplitude of the normalized electric field. (b) Electromagnetic simulation of a unit cell (array parameters: *s*=15 µm, *d*=25 µm.) showing the distribution of the Ez component of the electric field inside the patch microcavities at resonance for the degenerate TM_{10} and TM_{01} modes. (c) Simulated reflectivity spectra from a patch antenna microcavity array in the TM_{01} mode (top) and TM_{10} mode (bottom). The red curves correspond to the reflectivity spectra for the array configuration whose unit cell is presented in figure 1(b). Shaded gray lines correspond to reflectivity spectra for arrays with *s*=15 µm and wire lengths varying from *d*=10 µm to 40 µm. Blue lines represent the reflectivity spectra of a bare array (no wires), with array parameters: *s*=15 µm, and *d*=25 µm.

(c)-lower panel) as the field node is coincident with the wires. In contrast, the TM_{01} mode is coupled to the highly confining wires resulting in a higher quality factor (Figure 1 (c)-top panel). The wires are purely confining elements and do not radiate due to the canceling effect of the symmetric field distribution dictated by the neighboring microcavities. The enhancement of the quality factor is attributed to lower radiative losses from the wires, as previously reported for THz nano-antennas [23] and mid-IR detectors [24]. More importantly, the wires introduce a frequency shift of the TM_{01} mode, and by varying the length *d* of the wire one can design the detuning between TM_{01} and TM_{10} (Figure 1 (c)-top panel). For a given patch size, the TM_{10} resonant frequency is independent of the wire length and remains fixed at the resonant frequency Ω. Conversely, the spatial extension of the TM_{01} increases as the wire is made longer, shifting to lower frequencies, allowing one to control the detuning with respect to the TM_{10} mode.

In Figure 2, we show the typical optical and electrical properties of our devices. The device presented here has parameters *s*=15 µm and *d*=40 µm (see Supporting Information, Note 1 for characterization of devices with different configurations). In Figure 2 (a), we present the L-I-V characteristics obtained by driving the QCL in pulsed mode operation (repetition rate of 50 kHz, 10% duty cycle) at heat-sink temperatures of 10 K, 77 K, and 100 K (see Methods section for details about the characterization methods). The maximum peak optical power reaches 25 mW with a threshold current density J_{of}=270 A/cm^2, slope efficiency of ~111 mW A^{-1} and a wall-plug efficiency of 1.2%. (Measurements on a QCL fabricated in a double-metal ridge waveguide show similar threshold current densities as the patch array QCLs. See Supporting Information, Note 1 for details). All devices showed robust single mode operation over the entire current range as shown in Figure 2 (b).

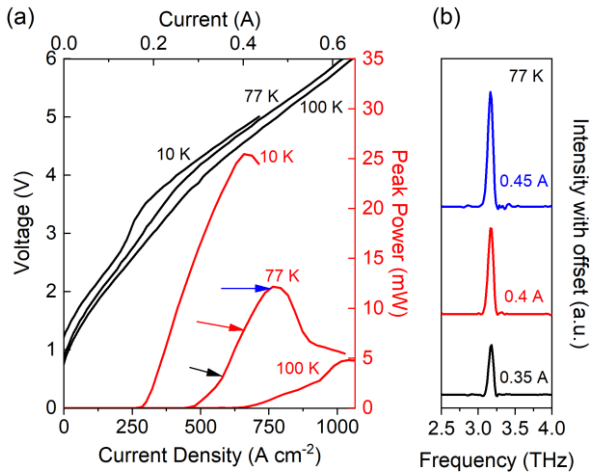

Figure 2. (a) Pulsed L-I-V characteristic of a device with patch sizes s=15 µm and periodicity p=55 µm (d=40 µm), measured at 10 K, 77 K and 100 K. (b) Emission spectra obtained at 77 K for various injection currents (indicated with colored arrows in L-I-V graph).

Next, we measured the far-field radiation pattern of the device at a heat sink temperature of 77 K at the maximum QCL peak power (see Methods section for details on the far-field measurements). We observe a clean beam with minimal parasitic background in Figure 3 (a). In Figure 3 (b) which shows a high-resolution scan, we measure a single-lobed Gaussian beam with a FWHM divergence angle as low as 2°x 2°. The measured far-field pattern is in excellent agreement with the simulated far-field pattern, presented in Figure 3 (c), calculated for a phase-locked array with the same geometrical parameters as the fabricated device. This observation confirms the phase-locking of the structure since the beam shaping arises from collective interference. Here, the phase-locking is ensured by the coupling with the plasmonic wires along the y- direction as well as other mutual coupling mechanism known in antenna arrays, such as surface waves [25, 26] and far-field global coupling [27].

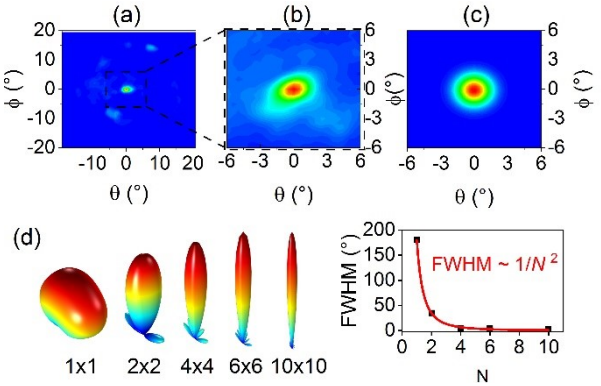

Figure 3. (a) Measured far-field intensity pattern of a 10x10 patch antenna microcavity array with a scanning range ±20° in both elevation and azimuthal directions. (b) High resolution (0.1°) far-field measurement. (c) Full wave finite element simulation of the far field intensity pattern for a 10x10 array. (d) Computed 3D far-field patterns for different planar arrays of NxN elements, and their respective FWHM divergence angles. In the graph, we show the associated calculated FWHM divergence fitted by a 1/N² function.

The main parameter impacting the divergence of the far-field radiation pattern is the number of resonators in the array, with no dependence on the array periodicity observed in the 10x10 array (see Supporting Information, Note 2 for a more detailed discussion based on antenna theory). As seen in Figure 3 (d), the radiated far-field pattern narrows from the ~180° single patch case to the 2°x2° divergence from a 10x10 array. We note the presence of low intensity side originating from the arraying (see Supporting Information, Note 3). For a planar array of NxN elements, the FWHM divergence follows an asymptotic behavior proportional to ~1/N^2 (see Supporting Information Note 4 for a discussion on extended arrays). For large arrays, this factor outweighs other parameters influencing the beam shape, such as the array periodicity (s+d). This allows the parameter d to be adjusted without affecting the quality of the far-field pattern.

Finally, we demonstrate an effective and coherent control of the polarization states by design of the array (see Supporting Information, Note 5). As mentioned earlier, the introduction of wires can be used to lift the degeneracy of the fundamental modes. The electric fields of the TM_{10} and TM_{01} modes oscillate in two perpendicular directions (along x- and y- direction, respectively). To select a specific polarization state, one has to consider how each mode resonance is tuned relative to the frequency of the QCL active region (Ω= 3.2 THz). A large detuning of one mode with Ω results in a linear polarization. A slight detuning of the modes with Ω allows one to adjust their respective losses and thus the relative emitted intensity along x and y to achieve an elliptical polarization. An overlap of the two modes leads to a circular polarization. By means of simulations, we identified the different combinations of design parameters s and d that enable the different regimes to be observed (see Figure 4 (d), (e), (f)) and we fabricated the corresponding devices. In Figure 4 (a), we show a device emitting a linearly polarized (~10:1) beam along the wire direction. An array with patch size s= 12 µm interconnected with wires of length d= 40 µm sets the TM_{01} mode at the resonant frequency Ω while shifting the TM_{10} mode to a region where no intersubband gain is present (see Supporting Information, Figure S4) as seen in Figure 4 (d). We obtained an elliptical polarization with the semi-major axis in the perpendicular direction by slightly detuning the TM_{10} and TM_{01} modes, as shown in Figure 4 (b). Lastly, we demonstrate circular polarization (Figure 4 (c)) in a device in which the mode degeneracy can be restored in resonance with Ω. To obtain a circular polarization, one needs to meet two conditions: same magnitude of the cross-polarized fields and a $\pi/2$ phase difference between them. These conditions are met for the device with s=15 µm and d=25 µm, which shows the cross-polarized emissions to be of equal magnitude (see Figure S3 in Supporting Information and Note 6) and providing a separation between resonators of $\lambda/4$, introducing a phase difference of $\pi/2$. For this case, we successfully measured a circular polarization achieving a degree of circular polarization ($DOCP = 2\sqrt{I_{max} \cdot I_{min}}/(I_{max} + I_{min})$) as high as 99%. (Evidence for the coherence of the polarization states is provided in Supporting Information, Note 5). We note that the beam shape is preserved for all the cases, confirming experimentally that the beam divergence depends essentially on the number of resonators forming the array, independent of its internal configuration.

In conclusion, we have demonstrated efficient THz surface-emitting lasers based on arrays of patch antenna microcavities with beam divergence as low as 2° x 2° by using the fundamental mechanism used for beam shaping in RF phased-arrays. We show that the beam quality is independent of the array geometry which can then be designed to define the polarization of the emitted radiation. Our device offers excellent flexibility and scalability as the monolithic architecture does not require complex lithographic processing, nor critical alignment, nor the use of external elements for its operation. Finally, our structure opens the way to realize a long-standing goal in the THz range: conceiving devices with high quality optical properties combined with advanced integrated functionalities with active control. Concretely, our architecture could be used to enable amplitude- or resonance detuning-based beam

steering [28, 29], and polarization control to achieve real-time tracking [30, 31] and polarization division multiplexing [32, 33] schemes in the THz, which would benefit future high-capacity wireless communications applications.

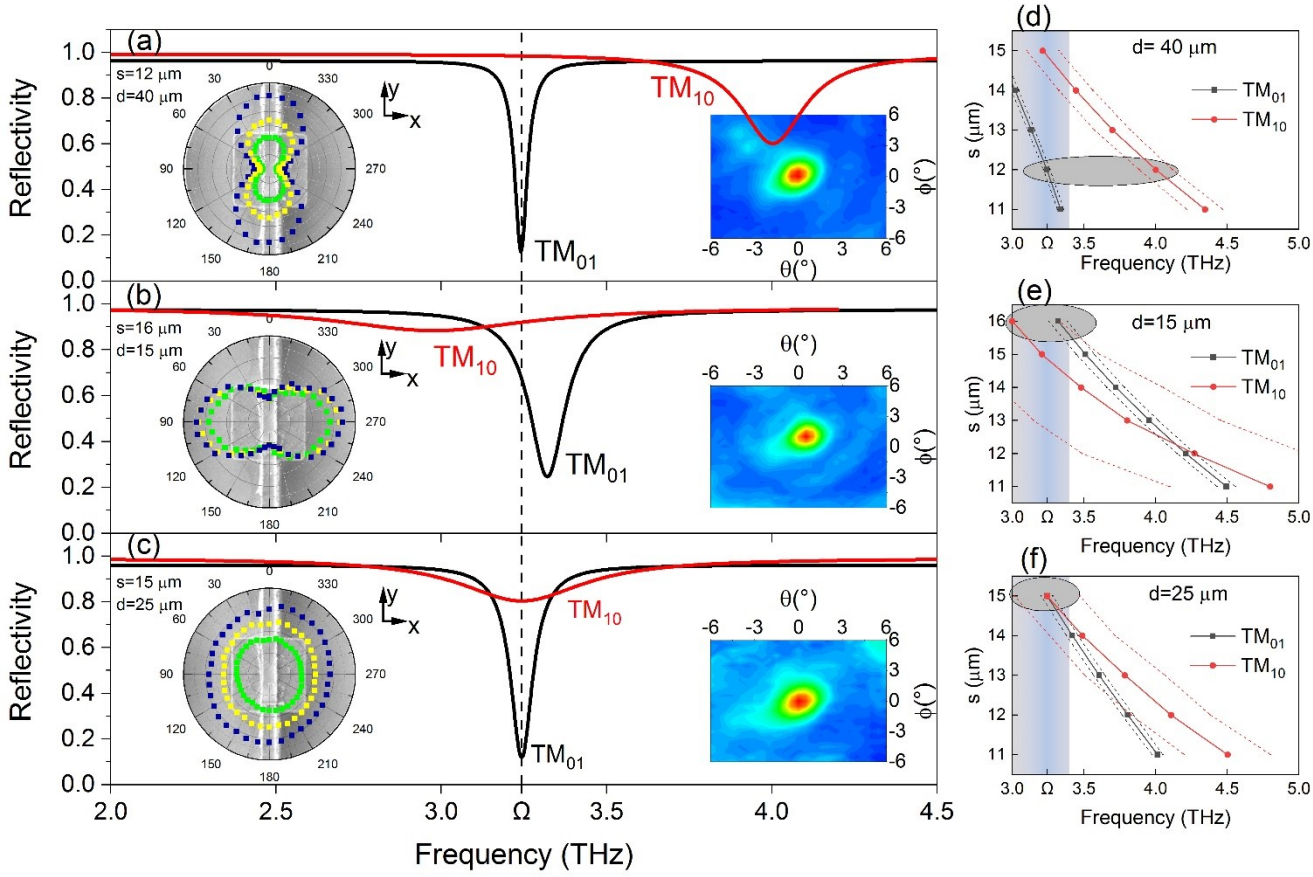

Figure 4. Reflectivity spectra (simulation), measured polarization state and measured far-field radiation pattern of samples with array parameters, (a) s= 12 μm, d=40 μm, (b) s=16 μm, d=15 μm and, (c) s=15 μm, d=25 μm. An SEM image of the top of a single wired patch microcavity is placed in the background of the polar plots to indicate the direction of the emitted THz signal relative to the patch structure. Polarization data were taken for three different pump currents (see corresponding L-I-Vs in Supplement 1, Section S2). (d) Map of the TM_{10} and TM_{01} resonant frequency peaks, obtained from reflectivity simulations, for arrays with different patch sizes s interconnected with wires of length d=40 μm. Distance between single points and dashed contours represents half the spectral FWHM for a specific (s, d) combination. Background blue colormap illustrates the gain of the QCL active region with its maximum located at Ω= 3.2 THz. Points highlighted in the gray oval indicate the fabricated and measured array. (e), (f) same as (d) for wire lengths d=15 μm and d=25 μm, respectively.

METHODS

Fabrication

The QC active region used in this study is based on a hybrid LO-phonon bound-to-continuum design [34, 35] . It comprises 85 periods of nine GaAs quantum wells, each composed of a GaAs/ Al0.15Ga0.85As heterostructure. A single period comprises **3**/9.5/**3**/11.8/**2**/12.9/**1**/16.2/**0.5**/10.1/**4**/14.5/**3**/17/**3**/7.1/**3**/8.6 (all in nm), where bold numbers refer to the thickness of the $Al_{0.15}Ga_{0.85}As$ barriers, and the underlined number denotes a Si-doped GaAs layer (3 x 10^{16} cm^{-3}). The active region was grown on a host GaAs wafer followed by a sacrificial $Al_{0.5}Ga_{0.5}As$ etch stop layer and a highly doped GaAs contact layer (2 x 10^{18} cm^{-3}). After the growth, Au-Au thermocompressive wafer bonding was performed to define the double metal structure. The host GaAs wafer was removed by mechanical lapping followed by wet etching. Removal of the etch stop layer followed by using HF selective wet etching. A first insulating layer for the contact pads was defined by UV-photolithography and vacuum sputter deposition of SiO_2 (200 nm). Next, arrays of patches and thin wires were defined by UV-photolithography and Ti/Au (10 nm/ 400 nm) lift-off. Finally, the patterned structures were used as a self-aligned mask to form the microcavities by dry-etching using inductively coupled plasma. The device was indium-soldered onto a copper mount and wire-bonded to external contact pads for electrical injection

Electromagnetic simulations

We performed full-wave three-dimensional electromagnetic simulations based on the finite-element method (FEM) by using the RF module of COMSOL Multiphysics. To obtain the reflectivity spectra, we modeled arrays with an air-box domain enclosing a wired-patch microcavity unit cell with Floquet periodic boundary conditions. An excitation port with TM polarization was placed at the top of the air-box to simulate a plane wave propagating in the z-direction. We used the complex refractive indices for gold and GaAs as in [36]. Quality factors, resonance frequencies and spectral FWHM were extracted by fitting the reflectivity spectra to a Lorentzian profile. To evaluate the far-field characteristics, we simulated finite array structures. To this end, 10x10 wired-patch microcavities were

placed in the center of an air hemisphere domain bounded by a perfectly matched layer (PML). Far-field calculations were performed in the boundary between the air sphere and the PML. As this model required significant computational resources, we performed parallel computation (MPI) on the HPC clusters of the Okinawa Institute of Science and Technology.

Electrical and optical characterization

All measurements were taken by mounting the device on the cold finger of a continuous flow cryostat. The cryostat is equipped with a polyethylene window with a measured transmittance of 83% in the 3-4 THz range. L-I-V curves were taken while driving the QCL at 50 kHz with a 10% duty cycle at heat sink temperatures of 10 K, 77 K and 100 K in a nitrogen-purged atmosphere. We utilized a Golay cell to detect the THz radiation from the device using a slow electrical modulation (15 Hz) for lock-in detection. Power levels were calibrated using a Thomas Keating absolute THz power meter. Peak power values are reported considering the transmittance of the cryostat window. No additional focusing optics were placed in between the QCL and power meter. For the spectra measurements of both patch arrays and ridge waveguides, we used a Fourier transform infrared spectrometer (FTIR)with a set of parabolic mirrors to collect the radiation from the QCLs and focus it into the focused input of the FTIR.

Far-field measurements

Measurements were performed in pulsed mode operation (50 kHz, 10% duty cycle) using a Golay cell with a small aperture mounted on a 2-axis spherical setup (θ, φ). The sample was scanned at a distance of 10 cm, covering a range of ±20° in both elevation and azimuthal directions with 1.0° angular resolution. A smaller window was then scanned at the center of maximum intensity with a ±6° range to acquire maps with higher resolution (0.3°). FWHM divergence values were found by extracting 1D cuts along θ and φ directions from the far-field intensity map and by fitting with Gaussian curves.

Polarization measurements

Data was taken at the center of the far-field radiation pattern by rotating a wire-grid analyzer in front of a Golay cell detector. An aperture was set in between the detector and the analyzer to collect only the FWHM of the THz beam.

ASSOCIATED CONTENT

Supporting Information

The Supporting Information is available free of charge on the ACS Publications website.

L-I-V characteristics of different patch antenna array configurations and double metal ridge waveguide THz QCLs. Notes on antenna theory (PDF).

AUTHOR INFORMATION

Corresponding Author

Julien Madéo – Femtosecond Spectroscopy Unit, Okinawa Institute of Science and Technology Graduate University, Okinawa, Japan.
Email: julien.madeo@oist.jp

Authors

Joel Pérez-Urquizo – Femtosecond Spectroscopy Unit, Okinawa Institute of Science and Technology Graduate University, Okinawa, Japan.

Yanko Todorov – Laboratoire de Physique de l'Ecole Normale Supérieure ENS, Université PSL, CNRS, Université de Paris, Sorbone Paris Cité Paris, France.
Lianhe Li – School of Electronic and Electrical Engineering, University of Leeds, Leeds, United Kingdom.
Alexander G. Davies – School of Electronic and Electrical Engineering, University of Leeds, Leeds, United Kingdom.
Edmund H. Linfield – School of Electronic and Electrical Engineering, University of Leeds, Leeds, United Kingdom.
Carlo Sirtori – Laboratoire de Physique de l'Ecole Normale Supérieure ENS, Université PSL, CNRS, Université de Paris, Sorbone Paris Cité Paris, France.
Keshav M. Dani – Femtosecond Spectroscopy Unit, Okinawa Institute of Science and Technology Graduate University, Okinawa, Japan.

Author Contributions

J.M., Y.T and C.S. conceived the devices. J.P.-U. fabricated the devices and performed the experiments. J.P.-U. and J.M. performed the numerical simulations. J.P.-U. and J.M. analyzed the data. L.L., A.G.D. and E.H.L. grew the MBE samples. J.P-U., J.M., Y.T. and C.S. interpreted the data. J.M supervised the project with the assistance of K.M.D. All authors contributed to discussions and manuscript preparation.

Notes

The authors declare no competing financial interests.

ACKNOWLEDGMENT

We thank OIST engineering support section and IT section for their support. E.H.L acknowledges support of the Royal Society and Wolfson Foundation. **Funding**: This work was supported by JSPS KAKENHI Grant number JP17K14126, the EPSRC (UK) programme grant 'HyperTerahertz' (EP/P021859/1) and in part by funding from the Femtosecond Spectroscopy Unit, Okinawa Institute of Science and Technology Graduate University.

REFERENCES

1. Lee, K. F.; Luk, K. M.; Lai, H. W., *Microstrip patch antennas*. World Scientific: 2017.
2. Mitra, R. N.; Agrawal, D. P., 5G mobile technology: A survey. *ICT Express* **2015,** *1* (3), 132-137.
3. Joshi, M. P.; Gond, V. J. In *Microstrip patch antennas for wireless communication: A review*, 2017 International Conference on Trends in Electronics and Informatics (ICEI), 11-12 May 2017; 2017; pp 96-99.
4. Todorov, Y.; Andrews, A. M.; Colombelli, R.; De Liberato, S.; Ciuti, C.; Klang, P.; Strasser, G.; Sirtori, C., Ultrastrong light-matter coupling regime with polariton dots. *Phys Rev Lett* **2010,** *105* (19), 196402.
5. Cui, T. J.; Qi, M. Q.; Wan, X.; Zhao, J.; Cheng, Q., Coding metamaterials, digital metamaterials and programmable metamaterials. *Light: Science & Applications* **2014,** *3* (10), e218-e218.
6. Grant, J.; Ma, Y.; Saha, S.; Khalid, A.; Cumming, D. R. S., Polarization insensitive, broadband terahertz metamaterial absorber. *Optics Letters* **2011,** *36* (17), 3476-3478.
7. Palaferri, D.; Todorov, Y.; Bigioli, A.; Mottaghizadeh, A.; Gacemi, D.; Calabrese, A.; Vasanelli, A.; Li, L.; Davies, A. G.; Linfield, E. H.; Kapsalidis, F.; Beck, M.; Faist, J.; Sirtori, C., Room-temperature nine-microm-wavelength photodetectors and GHz-frequency heterodyne receivers. *Nature* **2018,** *556* (7699), 85-88.
8. Palaferri, D.; Todorov, Y.; Chen, Y. N.; Madeo, J.; Vasanelli, A.; Li, L. H.; Davies, A. G.; Linfield, E. H.; Sirtori, C.,

Patch antenna terahertz photodetectors. *Applied Physics Letters* **2015,** *106* (16).
9. Perchec, J. L.; Desieres, Y.; Lamaestre, R. E. d., Plasmon-based photosensors comprising a very thin semiconducting region. *Applied Physics Letters* **2009,** *94* (18), 181104.
10. Delteil, A.; Vasanelli, A.; Todorov, Y.; Feuillet Palma, C.; Renaudat St-Jean, M.; Beaudoin, G.; Sagnes, I.; Sirtori, C., Charge-Induced Coherence between Intersubband Plasmons in a Quantum Structure. *Physical Review Letters* **2012,** *109* (24), 246808.
11. Chen, Y. N.; Todorov, Y.; Askenazi, B.; Vasanelli, A.; Biasiol, G.; Colombelli, R.; Sirtori, C., Antenna-coupled microcavities for enhanced infrared photo-detection. *Applied Physics Letters* **2014,** *104* (3), 031113.
12. McLean, J. S., A re-examination of the fundamental limits on the radiation Q of electrically small antennas. *IEEE Transactions on Antennas and Propagation* **1996,** *44* (5), 672.
13. Madéo, J.; Todorov, Y.; Sirtori, C., Antenna-coupled microcavities for terahertz emission. *Applied Physics Letters* **2014,** *104* (3).
14. Adam, A. J. L.; Kašalynas, I.; Hovenier, J. N.; Klaassen, T. O.; Gao, J. R.; Orlova, E. E.; Williams, B. S.; Kumar, S.; Hu, Q.; Reno, J. L., Beam patterns of terahertz quantum cascade lasers with subwavelength cavity dimensions. *Applied Physics Letters* **2006,** *88* (15).
15. Justen, M.; Bonzon, C.; Ohtani, K.; Beck, M.; Graf, U.; Faist, J., 2D patch antenna array on a double metal quantum cascade laser with >90% coupling to a Gaussian beam and selectable facet transparency at 1.9 THz. *Opt Lett* **2016,** *41* (19), 4590-4592.
16. Todorov, Y.; Sagnes, I.; Abram, I.; Minot, C., Purcell enhancement of spontaneous emission from quantum cascades inside mirror-grating metal cavities at THz frequencies. *Phys Rev Lett* **2007,** *99* (22), 223603.
17. Madéo, J.; Todorov, Y.; Gilman, A.; Frucci, G.; Li, L. H.; Davies, A. G.; Linfield, E. H.; Sirtori, C.; Dani, K. M., Patch antenna microcavity terahertz sources with enhanced emission. *Applied Physics Letters* **2016,** *109* (14).
18. Xu, L.; Chen, D.; Itoh, T.; Reno, J. L.; Williams, B. S., Focusing metasurface quantum-cascade laser with a near diffraction-limited beam. *Opt Express* **2016,** *24* (21), 24117-24128.
19. Curwen, C. A.; Reno, J. L.; Williams, B. S., Broadband continuous single-mode tuning of a short-cavity quantum-cascade VECSEL. *Nature Photonics* **2019,** *13* (12), 855-859.
20. Curwen, C. A.; Reno, J. L.; Williams, B. S., Terahertz quantum-cascade patch-antenna VECSEL with low power dissipation. *Applied Physics Letters* **2020,** *116* (24), 241103.
21. Madéo, J.; Pérez-Urquizo, J.; Todorov, Y.; Sirtori, C.; Dani, K. M., Engineering the Losses and Beam Divergence in Arrays of Patch Antenna Microcavities for Terahertz Sources. *Journal of Infrared, Millimeter, and Terahertz Waves* **2017,** *38* (11), 1321-1330.
22. Todorov, Y.; Tosetto, L.; Tessier, J.; Andrews, A. M.; Klang, P.; Colombelli, R.; Sagnes, I.; Strasser, G.; Sirtori, C., Optical properties of metal-dielectric-metal microcavities in the THz frequency range. *Opt Express* **2010,** *18* (13).
23. Feuillet-Palma, C.; Todorov, Y.; Vasanelli, A.; Sirtori, C., Strong near field enhancement in THz nano-antenna arrays. *Sci Rep* **2013,** *3*, 1361.
24. Miyazaki, H. T.; Mano, T.; Kasaya, T.; Osato, H.; Watanabe, K.; Sugimoto, Y.; Kawazu, T.; Arai, Y.; Shigetou, A.; Ochiai, T.; Jimba, Y.; Miyazaki, H., Synchronously wired infrared antennas for resonant single-quantum-well photodetection up to room temperature. *Nat Commun* **2020,** *11* (1), 565.
25. Khayat, M. A.; Williams, J. T.; Jackson, D. R.; Long, S. A., Mutual coupling between reduced surface-wave microstrip antennas. *IEEE Transactions on Antennas and Propagation* **2000,** *48* (10), 1581-1593.
26. Wang, C.; Li, E.; Sievenpiper, D. F., Surface-Wave Coupling and Antenna Properties in Two Dimensions. *IEEE Transactions on Antennas and Propagation* **2017,** *65* (10), 5052-5060.
27. Kao, T.-Y.; Reno, J. L.; Hu, Q., Phase-locked laser arrays through global antenna mutual coupling. *Nature Photonics* **2016,** *10* (8), 541-546.
28. Costas, J. P., An antenna beam steering technique comprised of constant-phase array elements. *Proceedings of the IEEE* **1981,** *69* (6), 745-747.
29. Johnson, M. T.; Siriani, D. F.; Tan, M. P.; Choquette, K. D., Beam steering via resonance detuning in coherently coupled vertical cavity laser arrays. *Applied Physics Letters* **2013,** *103* (20), 201115.
30. Amarasinghe, Y.; Mendis, R.; Mittleman, D. M., - Real-time object tracking using a leaky THz waveguide. **2020,** - *28* (- 12), - 18005.
31. Matsumoto, H.; Watanabe, I.; Kasamatsu, A.; Monnai, Y., Integrated terahertz radar based on leaky-wave coherence tomography. *Nature Electronics* **2020,** *3* (2), 122-129.
32. Li, X.; Yu, J.; Wang, K.; Zhou, W.; Zhang, J., Photonics-aided 2x2 MIMO wireless terahertz-wave signal transmission system with optical polarization multiplexing. **2017,** - *25* (- 26), - 33242.
33. Oshima, N.; Hashimoto, K.; Suzuki, S.; Asada, M., Terahertz Wireless Data Transmission With Frequency and Polarization Division Multiplexing Using Resonant-Tunneling-Diode Oscillators. *IEEE Transactions on Terahertz Science and Technology* **2017,** *7* (5), 593-598.
34. Scalari, G.; Hoyler, N.; Giovannini, M.; Faist, J., Terahertz bound-to-continuum quantum-cascade lasers based on optical-phonon scattering extraction. *Applied Physics Letters* **2005,** *86* (18).
35. Wienold, M.; Schrottke, L.; Giehler, M.; Hey, R.; Anders, W.; Grahn, H. T., Low-voltage terahertz quantum-cascade lasers based on LO-phonon-assisted interminiband transitions. *Electronics Letters* **2009,** *45* (20).
36. Palik, E. D., - Gallium Arsenide (GaAs). In *Handbook of Optical Constants of Solids*, Palik, E. D., Ed. Academic Press: Burlington, 1997; pp 429-443.

Authors are required to submit a graphic entry for the Table of Contents (TOC) that, in conjunction with the manuscript title, should give the reader a representative idea of one of the following: A key structure, reaction, equation, concept, or theorem, etc., that is discussed in the manuscript. Consult the journal's Instructions for Authors for TOC graphic specifications.

Insert Table of Contents artwork here

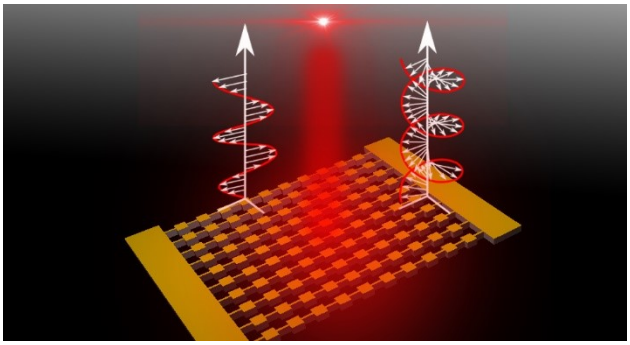

For Table of Contents Use Only

Monolithic patch-antenna THz lasers with extremely low beam di-vergence and polarization control.

Joel Pérez-Urquizo, Yanko Todorov, Lianhe Li, Alexander G. Davies, Edmund H. Linfield, Carlo Sirtori, Julien Madéo, and Keshav M. Dani.

Synopsis: Schematic of an array of patch antenna microcavities showing a collimated polarized THz beam.